International Journal of Nanomedicine

Dovepress
open access to scientific and medical research

Open Access Full Text Article

ORIGINAL RESEARCH

Calcium-Enriched Nanofibrillated Cellulose/ Poloxamer in-situ Forming Hydrogel Scaffolds as a Controlled Delivery System of Raloxifene HCl for Bone Engineering

Rabab Kamel[1]
Nahla A El-Wakil[2]
Nermeen A Elkasabgy[3]

[1]Pharmaceutical Technology Department, National Research Centre, Cairo, Egypt; [2]Cellulose and Paper Department, National Research Centre, Cairo, Egypt; [3]Department of Pharmaceutics and Industrial Pharmacy, Faculty of Pharmacy, Cairo University, Cairo, 11562, Egypt

Purpose: TEMPO-oxidized nanofibrillated cellulose (TONFC) originating from an agricultural waste (sugar cane) was utilized to prepare injectable in-situ forming hydrogel scaffolds (IHS) for regenerative medicine.

Methods: TONFC was prepared and characterized for its morphology and chemical structure using TEM and FT-IR, respectively. The cold method was applied to prepare hydrogels. Various concentrations of poloxamer 407 were added to the prepared TONFC (0.5%w/w). Different sources of calcium, Fujicalin (DCP) or hydroxyapatite (TCP), were used to formulate the aimed calcium-enriched raloxifene hydrochloride-loaded IHS. Gelation temperature, drug content, injectability and in vitro drug release were evaluated along with the morphological characters. Cytocompatibility studies and bone regeneration properties were assessed on Saos-2 cells.

Results: TEM photograph of TONFC showed fibrous nanostructure. The selected formulation "Ca-IHS4" composed of TONFC+15% P407+10% TCP showed the most prolonged release pattern for 12 days with the least burst effect (about 25% within 24 h). SEM microphotographs of the in-situ formed scaffolds showed a highly porous 3D structure. Cytocompatibility studies of formulation "Ca-IHS4" revealed the biocompatibility as well as improved cell adhesion, alkaline phosphatase enzyme activity and calcium ion deposition.

Conclusion: The outcomes suggest that Ca-IHS4 presents a simple, safe-line and non-invasive strategy for bone regeneration.

Keywords: nanofibrillated cellulose, raloxifene hydrochloride, calcium phosphate, in-situ forming hydrogel scaffolds, bone regeneration

Introduction

Recycling of agricultural wastes to be used as starting materials for biomedical applications can be a field of great interest from the economic as well as ecologic point of views.[1] Cellulose is one of the most abundant biopolymers originating from agro-wastes.[2] Researchers have produced TEMPO-oxidized nanofibrillated cellulose (TONFC) using different chemical and mechanical treatment methods. TONFC has possible medicinal applications due to its benign properties like safety, versatility, biodegradability and good mechanical properties with high surface area and low density.[1] The exploration of TONFC in regenerative medicine is well-reported due to its proliferative activity.[3,4] Also, due to the robust fiber network and high functionality; TONFC can control drug delivery.[5]

Correspondence: Nermeen A Elkasabgy
Faculty of Pharmacy, Cairo University, Kasr El-Aini Street, Cairo, 11562, Egypt
Tel +20 1141404144
Email nermeen.ahmed.elkasabgy@pharma.cu.edu.eg; nermeenadelahmed@outlook.com

Received: 9 June 2021
Accepted: 17 September 2021
Published: 5 October 2021

Graphical Abstract

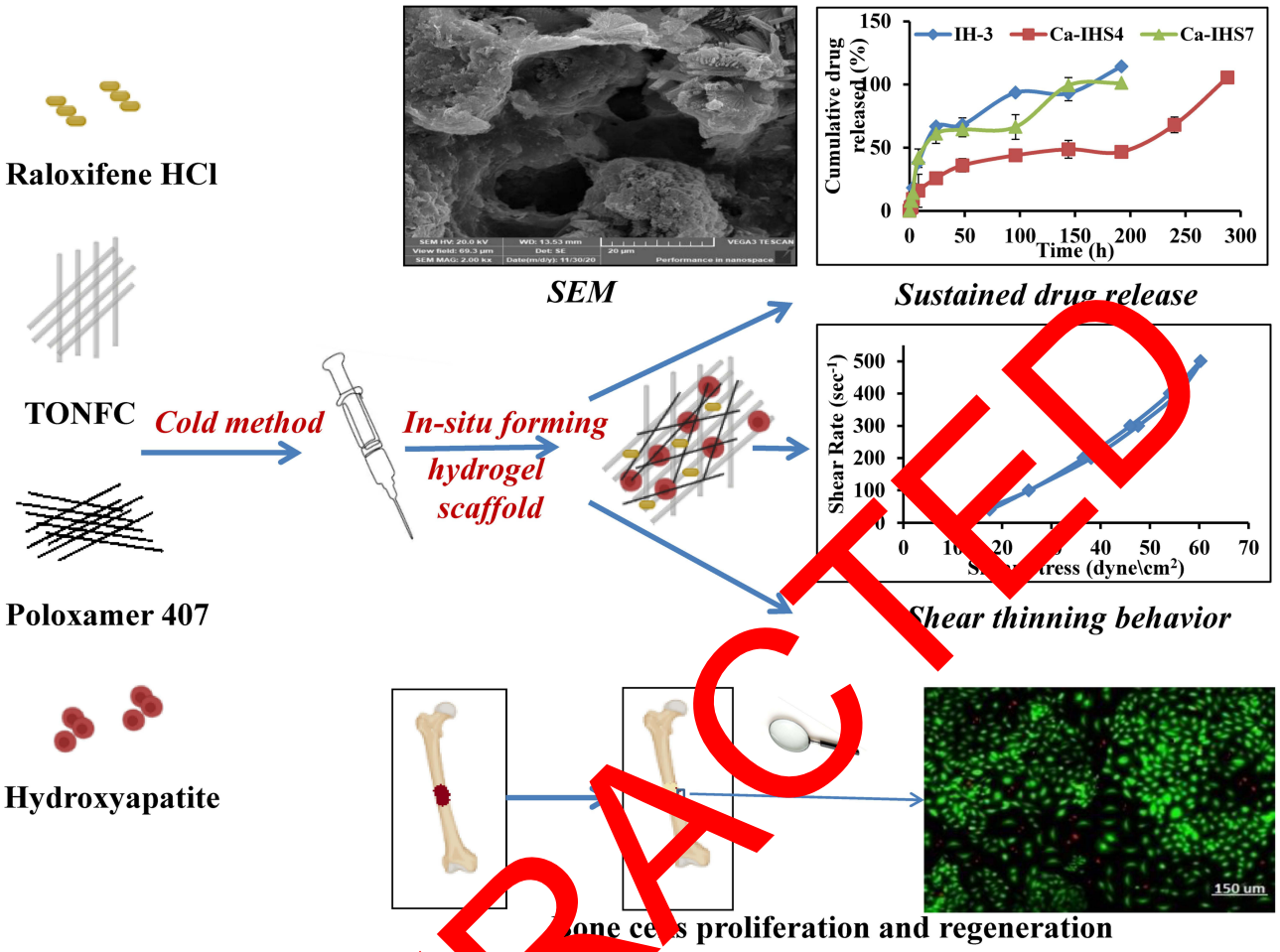

Natural bone has a complex bio-mineralized intricate hierarchical structure.[6] Bone defects caused by tumors, trauma or osteoporosis represent a serious health and socioeconomic problem. Biomaterials play a major role in the advancement of the tissue engineering area.[7] Nanobiomaterials have been discovered to mimic the extracellular matrix structure of bone tissues hence aiding in better cellular adhesion and proliferation.[8] Nanotechnology presents a major line in bone tissue engineering. Among the nanotechnological approaches with potential applications in bone tissue regeneration are: nanoparticles loaded with bioactive compounds (drugs, growth factors, etc.., nanoparticles used to label and lead stem cells to target sites as well as nanomaterials-based scaffolds.[9] Nanoparticles loaded with bioactive compounds can offer a good means for stabilizing the encapsulated molecules. More and above, they can facilitate the cell entry as well as control the drug release.[10,11] On the other side, several studies stated the success of nanoparticles like magnetic nanoparticles to label mesenchymal cells and track them in-vivo to the target tissue in a non-invasive manner.[12,13] In the same context, nanomaterials-based scaffolds represent an interesting approach to treat bone defects, where they combine the beneficial effects of nanomedicine as well as providing a suitable matrix, which serves as a matrix for better cellular adhesion and hence enhanced cell proliferation.[14] Also, the incorporation of nanoscale materials in scaffolds boosts the cellular adhesion as well as the combination and integration into the neighboring environment.[15] Blending of biomaterials with different characteristics can form tailor-made composites having the intended properties.[16]

An ideal bone scaffold must have the capability of promoting early mineralization and supporting new bone formation[17] while being biodegradable, non-immunogenic, biocompatible, with the ability to absorb liquids and to respond to development changes.[18–20] Also, for bone tissue engineering purposes, porous matrices are preferred to allow the cells migration, nutrient transport, tissue infiltration and vascularization.[4,21]

The use of injectable scaffolds seems to be an attractive approach because it diminishes the risk of infection and patient pain due to surgical intervention, decreases the scar formation as well as cost of treatment.[22] In order to assure the localized and prolonged effect of an injectable system, using in-situ forming delivery systems presents a remarkable approach. In-situ forming hydrogels are tailored 3D polymeric scaffolds with network structure capable of mimicking the extracellular matrix of the bone tissues. Owing to its distinctive structure, hydrogels can entrap bioactive molecules, which can be released in a controlled manner[23] as well as they can integrate with the surrounding tissues.[24] Thermo-sensitive Poloxamer 407 (P407) hydrogels can be considered as "smart" advanced drug delivery systems behaving as mobile liquids at room temperature that can be transformed into 3D semisolid gels at body temperature (37°C)[25,26] permitting efficient filling of any bone defect. After injection, P407 gels act as depots at the application site, increase drug residence time, prolong drug release leading to an improved drug bioavailability and efficacy.[27–31] Also, P407 is FDA approved for parenteral use due to its low toxicity.[32]

Raloxifene hydrochloride (RLX) is a selective estrogen receptor modulator (SERM) utilized in osteoporosis.[33] It has a low aqueous solubility as well as poor oral bioavailability (2%) due to severe first-pass metabolism.[34] Therefore, the "local" route of administration can be beneficial. In previous reports in literature, researchers have designed different RLX-loaded carriers for the local treatment of bone injury.[4,35,36]

Biominerals like calcium play a vital role in bone tissue restoration. Calcium maintains and organizes bone tissues and act as bone-building materials.[37] Calcium phosphates are widely used for bone regeneration as bones are composite tissues made up of collagenous, non-collagenous materials and minerals (eg, calcium phosphates).[38] Also, they affect angiogenesis and possess osteoconductive and osteoinductive properties,[39,40] besides being biocompatible and safe materials.[41] They may be manufactured in different solid or semisolid forms allowing wide area of application. Hydroxyapatite and some other calcium phosphates derivatives are the most frequently utilized calcium sources, thanks to their calcium/phosphorus (Ca/P) ratios similar to that of natural bone, in addition to their stability in the physiological environment.[42]

Merging calcium phosphate derivatives with different polymers for the preparation of scaffolds that simulate the composition of the bones offers a promising and an integrated line to combine the beneficial effects of inorganic and organic phases comprising the enhancement of mechanical characteristics as well as good bone-building properties.[43]

TONFC does not possess stimuli-responsive intrinsic gelling properties. Due to its tremendous benefits, this study aimed at using TONFC in combination with lower concentration of the smart polymer (P407) to successfully prepare injectable in-situ forming hydrogel scaffolds. Calcium-enriched systems were prepared in order to enhance the biological effect and to modify the flow properties of the TONFC/P407 systems in response to physiological stimulus. Two sources of calcium were used: Fujicalin®, dibasic calcium phosphate anhydrous (DCP), which is a spray-dried new grade of DCP with a higher specific surface area and porosity than the conventional one. It has a spherical shape with smooth surface with good flowing properties and blending capacity, which allows for uniformity of drug content and reduced variation.[44] Hydroxyapatite, tribasic calcium phosphate (TCP), is a biocompatible constituent of bone materials.[42] Formulations were assessed for their gelation temperature, drug content, injectability, in-vitro RLX release as well as their morphological characters. Determining the cytotoxicity on Saos-2 cells in addition to monitoring the cell adhesion besides alkaline phosphatase enzyme (ALP) and calcium ion concentrations were carried out to assess the bone mineralization process.

Although some recent studies were focused on the preparation of an injectable formulation based on cellulose nanofibers, to our knowledge this is the first study using sugar cane bagasse (an agro-waste widely spread in Egypt) to prepare TONFC-based medicated injectable thermoresponsive formulations enriched with the multi-function ingredient "calcium" acting as a scaffold reinforcing as well as bone-building agent.

Materials and Methods

Materials

Raloxifene hydrochloride (RLX) was purchased from Glochem Industries Limited (Hyderabad, Telangana,

India). Bleached bagasse pulp was gifted by Qena Company of Paper Industry, Egypt. Poloxamer 407, sodium bromide, sodium hypochlorite, hydroxyapatite (TCP; tribasic calcium phosphate) and 2,2,6,6-tetramethyl-piperidine-1-oxyl (TEMPO) were procured from Sigma Aldrich, St. Louis, USA. Fujicalin® (DCP; dibasic calcium phosphate anhydrous) was kindly donated by Fuji Chemical Industry CO., Ltd. (Toyama, Japan).

Human cells of bone osteosarcoma (Saos-2) with American type ATCC were obtained from Vacsera, Egypt. Sodium pyruvate and McCoy's 5a Medium supplemented with L-glutamine, penicillin G sodium, amphotericin B, streptomycin sulphate and fetal bovine serum were procured from Thermo Fisher Scientific, USA. Alkaline Phosphatase Assay Kit (Catalog Number, ab83369) was bought from Abcam, Cambridge, UK.

All other reagents were of analytical grade and the utilized water was distilled, deionized water.

Preparation of TEMPO Oxidized Nanofibrillated Cellulose (TONFC)

Tetramethyl pyridine oxyl (TEMPO)/sodium bromide/sodium hypochlorite were used to replace the OH group (C-6) of the COOH groups on the cellulosic chains.[45] In brief, the pulp suspension (pH 10) was mixed with 2 mmol/g sodium hypochlorite solution under magnetic stirring at 500 rpm (Stuart, SB162, UK) at 80°C. When the reaction is completed, 0.5 M HCl was dropped to almost neutralize the mixture. After attaining room temperature, the mixture was centrifuged (Centurion SCI, West Sussex, UK) at 9000 rpm to get rid of oxidizing agents. Neutrality was restored by repeated washing with deionized water. Dialysis of oxidized pulp (molecular weight cut-off 6–8 kD) against distilled water for 2 days was carried out. The oxidized suspensions were fibrillated utilizing ultrafine friction grinder Supermass colloider (model MKZA, disk model MKG-C 80, Masuko Sangyo Co., Ltd., Japan). Following, homogenization was conducted via Panther (model NS3006L, GEA NiroSoavi S.p.A., Italy) twice at 1000 and 1500 bar, sequentially.

Characterization of TEMPO Oxidized Nanofibrillated Cellulose (TONFC)

Determination of Carboxylic Content

The carboxylic content was assayed by the acid–base titration following TAPPI Test Method T237cm-98 (conductometric titrations) followed by acid/base titrations were conducted to determine the carboxylic content. TONFC (50 mg) were magnetically stirred with 0.01 M HCl (15 mL) at 125 rpm at ambient temperature, followed by titrating the resulting mixture against 0.01 M NaOH solution.

Morphological Examination

The prepared TONFC was scanned using TEM (Jeol, JEM-1230, Japan) to characterize its morphological properties. Drops from the suspension of the prepared TONFC were added onto a copper grid followed by staining using 2% (w/v) phosphotungstic acid. Post staining, the loaded copper grids were left to air dry then scanned at 200 kV.

Fourier Transform Infrared Spectroscopy (FT-IR)

FT-IR spectrum of the prepared TONFC was scanned employing FT-IR 8400 (Shimadzu, Kyoto, Japan). Samples were mixed with dry KBr followed by compressing the mixture into discs to be scanned from 4000 to 400 cm^{-1}.

Preparation of in-situ Forming Hydrogels Loaded with RLX

The hydrogels were formulated following the cold method[46,47] where Poloxamer 407(P407) was added, in different concentrations ranging between 10 and 30% w/v, to TONFC (0.5% w/w) under continual stirring at 1000 rpm. Then, the dispersions were reserved in refrigerator for 1 day. Calcium-enriched in-situ forming hydrogel scaffolds (Ca-HIS) were prepared by the addition of different concentrations of Fujiculin® (DCP) or hydroxyapatite (TCP) individually (5, 10 or 15% w/w) to the TONFC/P407 dispersion. Finally, the preparations were loaded with the drug (4 mg/g w/w) under stirring using Velp Scientifica magnetic stirrer (Europe) until uniform mixtures are formed. The composition of the formulations is compiled in Table 1.

Gelation Temperature

The sol–gel transition behavior of the hydrogels was assessed visually following the tube inversion method.[48,49] Certain volumes (2 mL) were transferred into tightly closed test tubes at room temperature; subsequently, the temperature was gradually increased. The gelation temperature was considered as the temperature at which no flowing occurs (within 1 min) after tilting the tubes to an angle of 90°. Successful preparations behaving as "sol" at room

Table 1 Composition and Characterization of the Investigated Formulations

Formulation Code	Formula Composition	Sol-Gel Behavior at Different Temperatures		Flow Rate (mL/min)
		25 °C	37 °C	
IH-1	TONFC + 10% P407	Sol	Sol	–
IH-2	TONFC + 15% P407	Sol	Sol	–
IH-3	TONFC + 20% P407	Sol	Gel	0.42 ± 0.01
IH-4	TONFC + 25% P407	Gel	Gel	–
Ca-IHS1	TONFC + 10% P407+5% TCP	Sol	Sol	–
Ca-IHS2	TONFC + 10% P407+10% TCP	Sol	Viscous solution	–
Ca-IHS3	TONFC + 15% P407+5% TCP	Sol	Viscous solution	–
Ca-IHS4	TONFC + 15% P407+10% TCP	Sol	Gel	0.50 ± 0.06
Ca-IHS5	TONFC + 10% P407+5% DCP	Sol	Viscous solution	–
Ca-IHS6	TONFC + 10% P407+10% DCP	Sol	Viscous solution	–
Ca-IHS7	TONFC + 15% P407+5% DCP	Sol	Gel	0.36 ± 0.01
Ca-IHS8	TONFC + 15% P407+10% DCP	Sol	Gel	0.35 ± 0.02

Note: All formulations were prepared using 0.5% w/w TONFC and loaded with 4 mg/g RLX.

temperature and shifting from "sol" to "gel" behavior at 37°C were subjected to further investigation.

Characterization of the Prepared in-situ Forming Hydrogels Loaded with RLX

Drug Content

Certain volumes of the investigated hydrogels corresponding to 2 mg RLX were placed separately to 250 mL volumetric flask. Following, the drug was extracted with 100 mL 0.1% w/v of Tween® 80 using Ultrasonic bath sonicator (Model SH 150-41, PCI Analytics Pvt. Ltd. Mumbai, India) for 24 h. After appropriate dilution of the withdrawn aliquots, the drug was analyzed at 285 nm using Shimadzu UV Spectrophotometer (1601/PC, Kyoto, Japan). The drug content was calculated as follows:

$$\%\,\text{Drug content} = \left(\frac{\text{Actual amount of the drug in hydrogel}}{\text{Initial amount of the drug}}\right) \times 100 \quad (1)$$

Rheological Properties

The rheological characteristics of the examined samples were assessed conducting the cone and plate rheometer (Brookfield DV3THB cone/plate rheometer, spindle CPE-40 and RheocalcT software, v 1.1.13 software). A volume of 1.5 mL of the sample was put into the rheometer plate and then exposed to a gradual shear rate rise from 20 to 500 sec^{-1}. The processing temperature of the apparatus was maintained at 25±2°C using a water bath (PolyScience model 9006, USA).

Farrow's equation was applied to indicate the flow behavior of the formulations by illustrating log of the shear stress against log of the shear rate values and calculating Farrow's constant:[50]

$$\text{Log } D = N \text{ Log } S - \text{Log } \eta, \quad (2)$$

where D is the shear rate (s^{-1}), S is the shear stress (Pa), N is Farrow's constant and η is the viscosity (Pa.s). Different types of flow were determined according to the N value. N values = 1 indicate Newtonian flow, values <1 refer to shear thickening flow and values >1 indicate shear thinning flow.

Determination of Injectability

The simplicity and easiness of the injectability of the investigated formulations in comparison to the market oily product; Betolvex™ was assessed utilizing a modified home-made device[35,36] to that formerly reported in the literature.[51] Briefly, 1 mL of investigated samples was transferred individually to a 3-mL syringe attached to 21 gauge needle. Then, a rubber tube previously connected to an air pump was fixed at the back of the syringe. Air was applied on the liquid surface after switching the air pump, and the pressure on liquid surface was measured and preserved at 70 mmHg using a sphygmometer. Injectability was compared by assessing the required time to release the 1 mL sample as well as by calculating the flow rate (mL/min).

In-vitro Release Studies

The dialysis bag technique was used to assess the in-vitro drug release from the tested hydrogel formulations.[52] Accurately measured volumes of the tested hydrogel loaded with 2 mg RLX was transferred to cellulose

dialysis bags; soaked in distilled water overnight previously. After securing the dialysis bags at both ends; they were transferred to glass bottles containing 90 mL of 0.1% w/v Tween® 80 solution in distilled water. The bottles were placed in an incubator shaker (Unimax, IKA, Germany) operated at 90 strokes/min at 37 ± 0.5°C. Withdrawn aliquots were replaced with fresh release medium and then evaluated for drug content spectrophotometrically at 285 nm.

The release data were analyzed by linear regression analysis and fitted to Korsmeyer–Peppas model[53,54] to calculate the release rate constant (K) and time necessary for the release of 50% and 90% of the drug (t_{50} and t_{90}, respectively). Also, the release kinetic model was determined by calculating release exponent value (n-value).

Characterization of the Chosen in-situ Forming Hydrogels Loaded with RLX

X-Ray Diffraction (XRD)

The chosen formulation and its individual constituents; RLX, TONFC, P407 and TCP were analyzed using Shimadzu x-ray diffractometer (XD-610, Kyoto, Japan). Irradiation of the samples with Ni, Cu Kα radiation at 40 kV and 20 mA was carried out; then, samples were scanned at 2º/min from 3 to 60º (2θ).

For comparison purposes, the crystallinity index (CI) was determined applying the peak height method and calculated using Segal empirical formula:

$$CI(\%) = (I_{002} - I_{AM})/I_{002} \times 100\%, \quad (3)$$

where I_{002} is the peak intensity relative to the crystalline cellulose I (2θ = 22°) and I_{AM} is the minimum intensity between both 002 and 110 peaks (2θ = 18°).

Scanning Electron Microscope (SEM)

The morphological structure of the formed air-dried hydrogel scaffold after being soaked in phosphate buffer pH 7.4 for 7 days was assessed using SEM (JSM-6400; JEOL Ltd., Tokyo, Japan) equipped at 5–10 kV. Tested samples were coated with gold by a sputter coater system (Edwards Sputter Coater, UK).

Cytocompatibility Studies

Cell Line Culture

Saos-2 cells were incubated with McCoy's 5a culture medium contained in T75 culture flasks (Corning®, USA). McCoy's 5a culture medium supplied with 2 mM L-glutamine, 100 units/mL penicillin G sodium, 250 ng/mL amphotericin B, 100 units/mL streptomycin sulphate, and 10% fetal bovine serum was used to grow human bone osteosarcoma cells (Saos-2). The culture medium was transferred to T75 culture flasks (Corning®, USA) and Saos-2 cells were seeded on it in a humidified air (95%) saturated with 5% CO_2 at 37°C and kept for 72h in Corning® 96-well tissue culture plates till reaching a concentration of 5×10^4 cell/well.

Assessment of Cytotoxicity Applying the Viability Assay

The metabolic activity of the viable cells was assessed by MTT (3-(4,5-dimethylthiazol-2-yl)-2,5-diphenyltetrazolium bromide) assay. Incubated Saos-2 cells in 96-well tissue plates were co-cultured with samples (equivalent to 6.25, 12.5, 25, 50, 100, 150 or 200 µg/mL drug) of the hydrogel or the drug suspension and compared to the control (untreated cells; cells receiving only the medium without the addition of the tested samples).

The assay was carried out for a total of 21 days, where assessment of the viable cells count was recorded at 3 points: 7, 14, and 21 days post incubation. MTT (10 µL from 12 mM in phosphate buffer saline; pH 7.4) were added to the investigated well plates and incubated for 4 h at 5% CO_2 at 37°C. Following, 50 µL DMSO was added and kept on every single well for 10 min at 37°C in advance of counting the viable cells. The optical density at 550 nm was analyzed by a microplate reader (680 XR reader, BIORAD, Hercules, CA, USA), and the % viability for every well was calculated relative to the control.

Cell Growth Pattern

Saos-2 cells were incubated with the examined hydrogels for 3 weeks in 8-chamber cell culture slides (5 x 10^4cells/chamber, SPL Life Sciences, Korea), then stained with nucleic acid binding dye; acridine orange (100 µg/mL in phosphate buffered saline pH 7.4) and observed under fluorescence microscopy (Axio Imager Z2, Zeiss, Goettingen, Germany). A digital camera (Axio Cam MRC3 S/N 4299) was applied to capture photos at 7, 14 and 21 days.

Alkaline Phosphatase Assay

Alkaline Phosphatase Assay Kit was used to determine the concentration of ALP enzyme through a calorimetric assay, which depends on the formation of a yellow color due to the conversion of p-nitrophenyl phosphate (pNPP) to the dephosphorylated form (p-nitrophenol; pNP) by the ALP.[56]

The standard calibration curve was constructed using different pNPP serial dilutions (0, 2, 4, 8, 12, 16 nM/well) in 96 well plates mixed with 10 µL of ALP standard solution. The reaction was maintained at 25°C for duration of 1h before adding 20 µL of ALP stop solution. Finally, the concentration of the yellow color (pNP) was monitored by measuring its absorbance at 405 nm utilizing a micro-plate reader.

The examined samples were incubated with Saos-2 cells independently in 8-chamber cell culture slides (5×10^4 cells/chamber) for 3 weeks and the ALP action was monitored after 7, 14 and 21 days post incubation. After each investigation time point, the incubated cells were washed with assay buffer and homogenized (Heidolph Instruments, Germany) then centrifuged (Model 8880, Centurion Scientific Ltd., W. Sussex, UK) at 13,000g for 5 min. Certain volume from the supernatant (80 µL) was mixed with the stop solution (20 µL) in a 96-well plate, then pNPP stock solution (50 µL) were put on the examined samples and control. ALP activity was evaluated as follows:

$$\text{ALP activity} = (B/\Delta T x V) \times D, \quad (4)$$

where, B represents the amount of pNP (µmol), ΔT is the reaction time (min), V is the real sample's volume (mL) and D is the dilution factor.

Calcium Ion Concentration Assay

Calcium Colorimetric Assay Kit was utilized to determine calcium ion concentration through the formation of the chromogenic complex between calcium ions and the chromogenic agent (o-cresolphthalein). Both the complex and calcium ions concentrations are directly proportional.

A standard calibration curve was constructed using several serial dilutions of calcium ions 0.4, 0.8, 1.2, 1.6 and 2.0 µg calcium/well in the 96 well plate.

The same incubation procedures of Saos-2 cells with the samples were followed as in the ALP test for 21 days. In brief, 90 µL of o-cresolphthalein were introduced into the wells containing the samples or the control mixed in advance with 60 µL calcium assay buffer, then the wells were kept for 10 min at ambient temperature. The calcium ion concentration was analyzed at 575 nm by a microplate reader and calculated.

Statistical Analysis

The collected results were represented as mean ± standard deviation (n=3). The results were statistically analyzed using one-way analysis of variance (one-way ANOVA) and Least Significant Difference (LSD) test. SPSS® software (version 16, SPSS Inc., Chicago, USA) was used for statistical interpretations. Differences with p-values <0.05 were significant.

Results and Discussion

Characterization of TEMPO Oxidized Nanofibrillated Cellulose (TONFC)

Determination of Carboxylic Content

The calculated carboxylic content was found to be 0.91 mmol/g.

Morphological Examination

TEM micrograph (Figure 1) shows the fibrous network structure of the prepared TONFC. Additionally, the obtained TONFC showed was 10–20 nm in diameter and several microns in length, which offers TONFC special morphology.

Fourier Transform Infrared Spectroscopy (FT-IR)

FT-IR is a reliable tool for rapid and easy identification of polymers like TONFC. Figure 2 represents the FT-IR spectrum of the prepared TONFC showing its characteristic peaks. A peak due to its OH group vibration as well as CH group stretching could be observed at 3417.9 and 2920.9 cm^{-1}, respectively. Moreover, the successful TEMPO oxidation of –OH to –C=O at C-6 might be confirmed by the appearance of a peak at 1612.5 cm^{-1}.

Preparation of in-situ Forming Hydrogels Loaded with RLX and Investigation of Gelation Temperature

A good scaffold should provide a 3D structure supporting cell adhesion and proliferation. To meet these multiple needs, this necessitates the fabrication of hybrid scaffolds

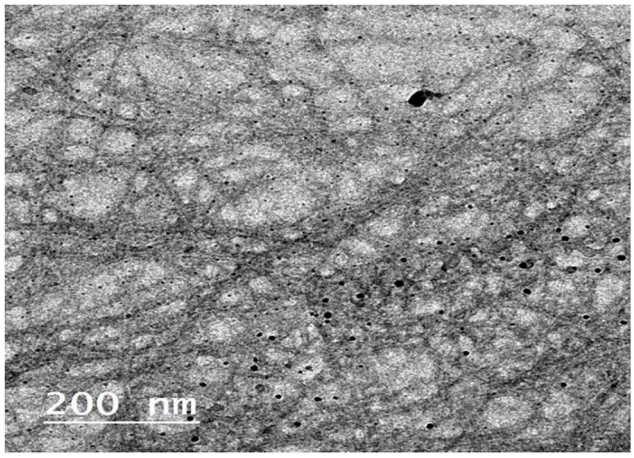

Figure 1 TEM photograph of TONFC showing the fibrous nanostructure.

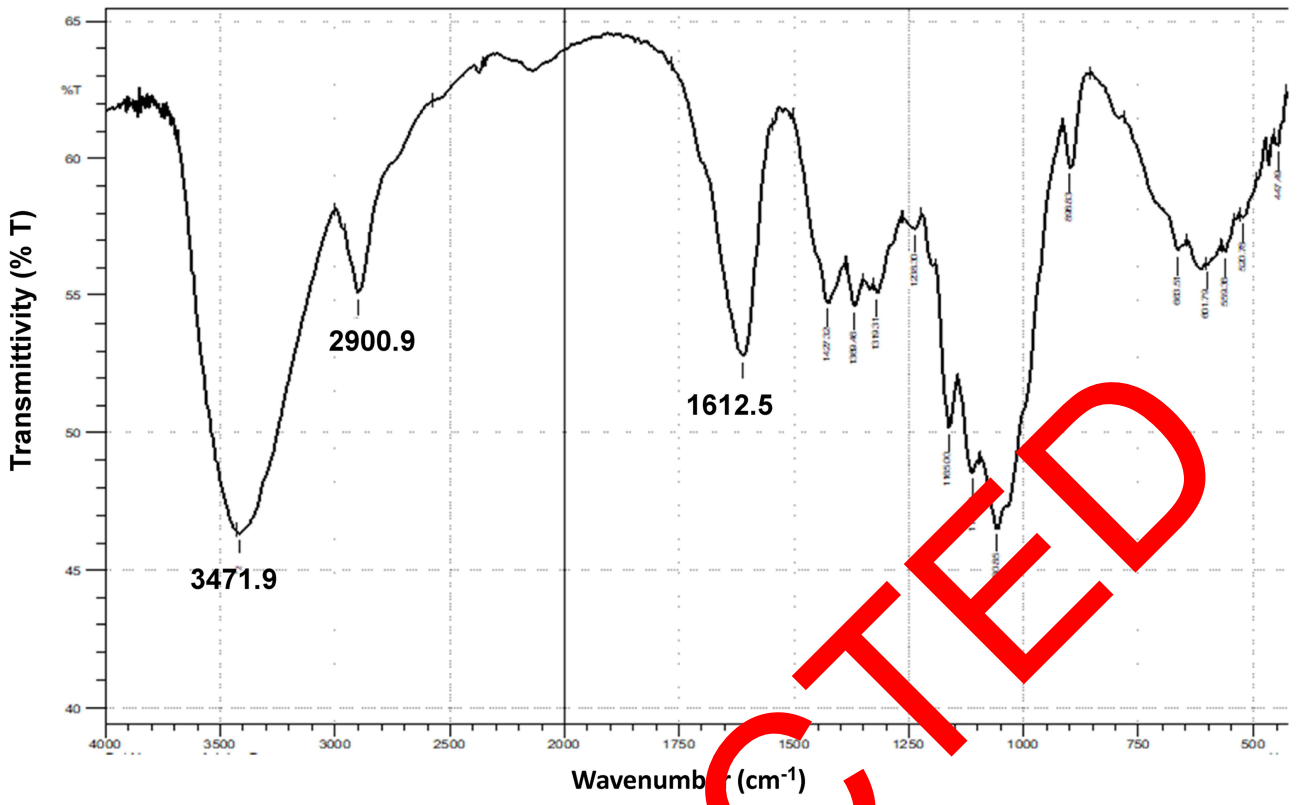

Figure 2 FT-IR of the prepared TONFC. The peaks due to OH group vibration and CH group stretching could be detected at 3417.9 and 2900.9 cm^{-1}, in that order. A peak appearing at 1612.5 cm^{-1} might indicate the successful oxidation of –OH present at C6 to –C=O.

made up of more than a single component. In this study, the combination of different materials with different properties was aimed through the fabrication of calcium-enriched in-situ forming hybrid hydrogel scaffolds made up from TONFC, P407 and either DCP or TCP. In-situ forming scaffolds provide an appealing alternative to traditional surgical interventions. Additionally, they can be fabricated easily requiring few steps and equipment.

Table 1 shows the behavior of TONFC/P407 hydrogels loaded with RLX. At a concentration of 20% w/w, P407 was capable of forming a formulation acting as gel at body temperature while behaving as liquid at room temperature; while at lower P407 concentrations the formulations failed to make a gel at 37°C. On the other hand at a higher P407 concentration (25% w/w), drug loaded TONFC/P407 formulations behaved as gel at both room and body temperature. The targeted thermo-responsive in-situ hydrogels subjected to further investigations are those having a gelation temperature more than ambient temperature so that they can be transformed to gel post injection at the application site where the temperature is 37°C.

The formation of injectable hydrogel scaffolds necessitates that the constituents solidify as a 3D matrix in the body fluids physiological conditions within a short period of time. Additionally, the stability of the resultant scaffolds is a crucial factor. The preparation of calcium-enriched formulations can allow forming non-decaying scaffolds[57] while decreasing the concentration of P407 needed to initiate the in-situ gelation. As seen in Table 1, for the calcium-enriched formulation, at a P407 concentration of 10% w/w, all the formulations failed to form gels at body temperature. By using a P407 concentration of 15% w/w, addition of 10% w/w of the calcium source (TCP) as well as addition of 5% or 10% w/w of the calcium source (DCP) allowed to obtain a strong gel at body temperature while behaving as liquid at room temperature, these gels will be subjected to the following examinations.

Characterization of the Prepared in-situ Forming Hydrogels Loaded with RLX

Drug Content

All the examined formulations had elevated % drug content values. The values were 93.10±0.81, 105.59±6.20, 101.15±6.32 and 90.45±1.34 for IH-3, Ca-IHS4, Ca-IHS7 and Ca-IHS8, respectively. High values indicated

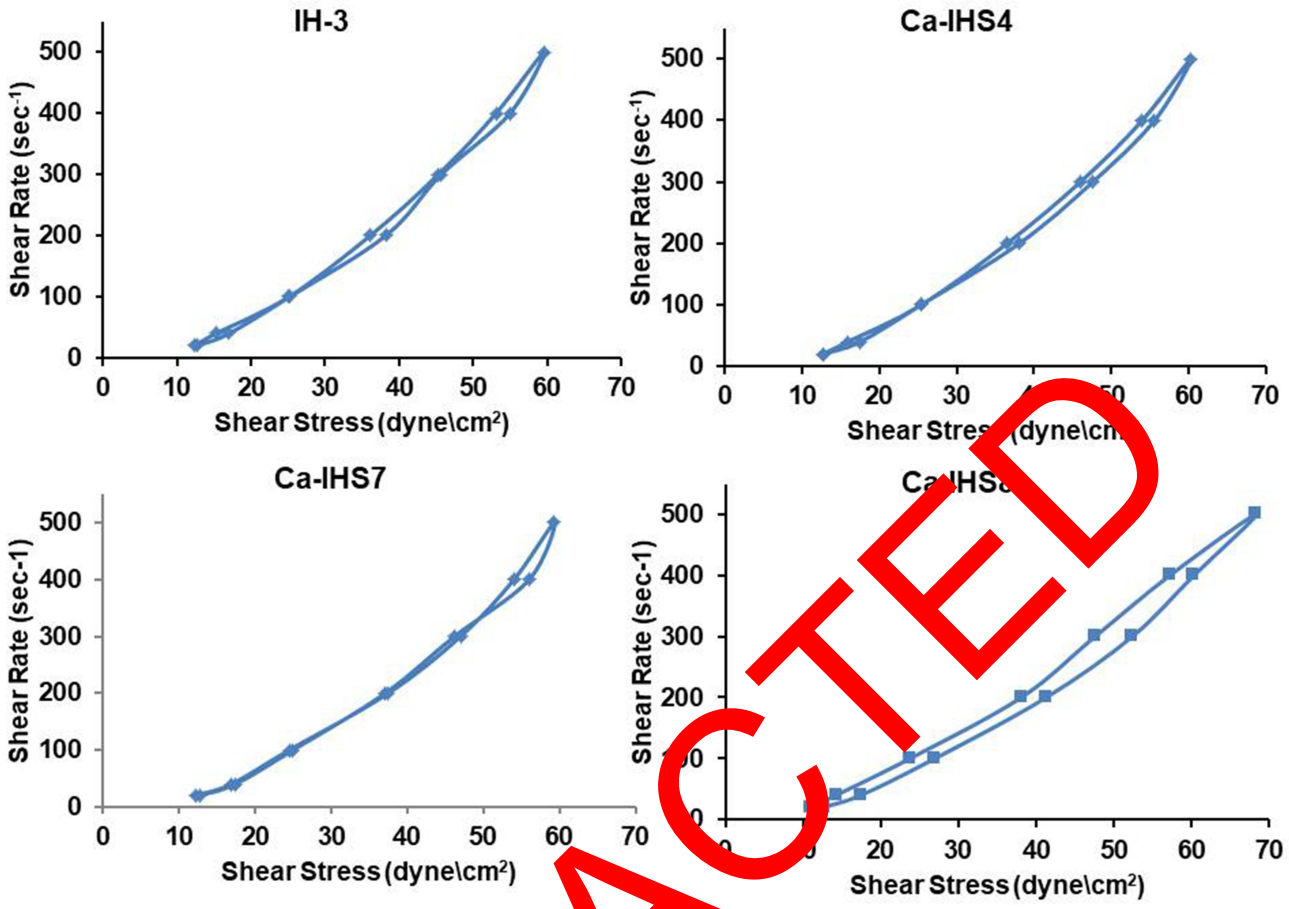

Figure 3 Relation between the shear stress and shear rate of formulations IH-3, Ca-IHS4, Ca-IHS7 and Ca-IHS8. The tested formulations possessed shear thinning behavior with N values >1.

the appropriateness of the preparation method along with the formulation parameters, which reduced the drug loss and permitted for the uniformity of drug content.

Rheological Properties

Viscosity of fluids gives an indication about the resistance to shape deformation. Newtonian fluids possess constant viscosity values while non-Newtonian fluids have different viscosity values when applied force overtime.[58] The flow behavior of the tested formulations represented as the relation between the shear stress and the shear rate is illustrated in Figure 3. It could be observed that all the examined formulations (IH-3, Ca-IHS4, Ca-IHS7 & Ca-IHS8) possessed shear thinning behavior with N values >1, where the calculated values were 1.99, 2.01, 2.02 and 1.79, respectively.

Determination of Injectability

A prerequisite for a successful parenteral preparation is to be injectable using a suitable syringe. The injectability of the examined hydrogels (IH-3, Ca-IHS4, Ca-IHS7 & Ca-IHS8) was judged by calculating their mean flow time and rate.[59] All the investigated formulations possessed significantly lower flow time and higher flow rate ($p < 0.05$) compared to the market oily injection; Betolvex™ under the same pressure except for formulation Ca-IHS8 (TONFC + 15% P407+10% DCP) which showed non-significant difference ($p > 0.05$) with Betolvex™. Moreover, no significant change ($p > 0.05$) could be observed between the three formulations (IH-3, Ca-IHS4 & Ca-IHS7). The low flow rate of formulation Ca-IHS8 might be attributable to using high concentrations of DCP (10% w/w). By comparing the mean particle size of DCP with TCP, it could be noticed that DCP has a higher mean particle size of 115 μm[44] versus 10 μm for TCP.[60] It was previously stated that the increase in particle size of calcium phosphate might hinder the injectability.[61–63] The obtained flow rate values of IH-3, Ca-IHS4, Ca-IHS7 & Ca-IHS8 were 0.42 ± 0.01, 0.50 ± 0.06, 0.46 ± 0.01 and 0.30 ± 0.02 mL/min, respectively, in comparison to Betolvex™ (0.29 ± 0.01 mL/min).

Table 2 Release Data of the Prepared Formulations Loaded with RLX

Formulation Code	Release Data Kinetics According to Korsmeyer–Peppas Model			
	Release Rate[a] (K; %/h)	t_{50}[b] (h)	t_{90}[c] (h)	n-Value[d]
IH-3	7.30 ± 0.05	10.00 ± 0.14	18.45 ± 0.17	0.65 ± 0.01
Ca-IHS4	3.37 ± 0.04	26.24 ± 0.18	47.52 ± 0.16	0.56 ± 0.01
Ca-IHS7	7.82 ± 0.60	10.82 ± 0.79	20.16 ± 1.78	0.55 ± 0.02

Notes: [a]K: release rate constant. [b]t_{50}: time required for the release of 50% of the drug. [c] t_{90}: time required for the release of 90% of the drug. [d] n-value: release exponent. Each value represents the mean ± SD (n=3).

From the above results, it can be concluded that the following composites (IH-3, Ca-IHS4 and Ca-IHS7) possessed higher flow rates and hence were more convenient as injectable systems, hence were subjected for release studies.

In-vitro Release Studies

Release studies were carried out for 12 days targeting a prolonged therapeutic action of the prepared formulations. Almost 85% of RLX was released within 3 h in case of the drug suspension, confirming the appropriateness of the release method and the used dialysis membrane.

Table 2 presents the effect of different formulation factors on K, t_{50}, t_{90} and n-value for comparison purposes.

As demonstrated in Figure 4, it can be noticed that formulation Ca-IHS4 prepared using 10% TCP presented a more controlled release pattern with reduced burst release ($p < 0.05$) with only 25% drug release compared to the other formulations, which showed the release of more than 60% within the first 24 h. Also, the release in case of Ca-IHS4 was extended up to 12 days; this retardation in drug release can be due to the presence of TCP in a sufficient amount on the surface and within the matrix of the hydrogel.[64]

By relating the release data of Ca-IHS4 with the other formulations (IH-3 and Ca-IHS7), it could be noticed that it possessed lower K and higher t_{50} and t_{90} values ($p<0.05$) which might be enforsed to the use of higher amounts of TCP (10% w/w). Additionally, the lower solubility of TCP in comparison to DCP[65] might explain the more sustained release behavior obtained with formulation Ca-IHS4. Hence, formulation Ca-IHS4 was elected for further studies.

By comparing the release exponent values (n), it could be observed that all the investigated samples possessed n-values ranging between 0.55 ± 0.02 and 0.65 ± 0.01 indicating anomalous transport, which is a result of a combination between diffusion and erosion controlled drug release.[66]

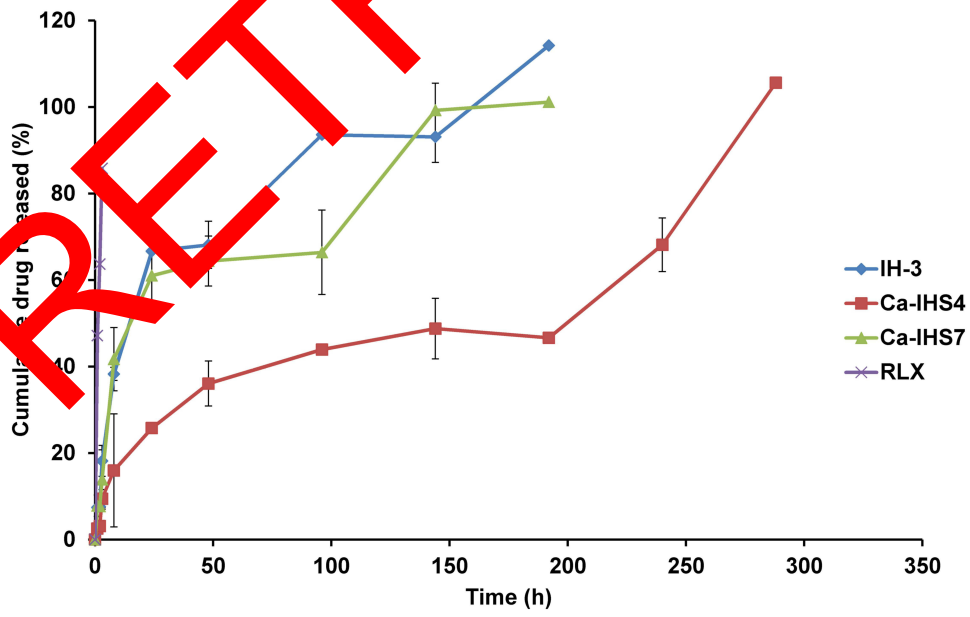

Figure 4 Release profiles of RLX from the prepared formulations. Formulation Ca-IHS4 showed the most controlled release pattern with reduced burst release of about 25% within 24 h compared to the other investigated formulations ($p < 0.05$). Additionally, formulation Ca-IHS4 had lowest k and higher t_{50} and t_{90} values ($p<0.05$). The release of RLX from formulation Ca-IHS4 was extended up to 12 days.

As explained above, the mixed TONFC/P407 matrix can provide numerous advantages. The thermoresponsive properties of TONFC/P407 matrix using a lower concentration of P407 compared to a matrix composed of P407 alone can be due to the interconnecting network formed between the active groups of both polymers supported by the fibrous structure of TONFC which can present the "backbone" of the preparation.

Characterization of the Chosen in-situ Forming Hydrogels Loaded with RLX

X-Ray Diffraction (XRD)

The XRD patterns of Ca-IHS4 as well as its constituents are represented in Figure 5. The XRD of the drug shows ten peaks, over the range 13–31° (2θ), of different intensities, including three sharp and intense peaks demonstrating its crystalline mode. The diffraction pattern of TONFC shows the principle peaks of cellulose I at 2θ = 22.3°, which is due to 002 crystalline plane and the peaks at 2θ = 16.3° and 22.5° are assigned to reflection of the amorphous 110 and $1\bar{1}0$ lattice planes.[67] TONFC has both amorphous and crystalline domains; this semi-crystalline nature is confirmed by the crystallinity index (CI) of 76%. The XRD of P407 identifies its semi-crystalline nature due to two sharp peaks at 18.7° and 22.8° in addition to some broad low-intensity peaks (2θ). In the same context, TCP shows several characteristic peaks at 25.6, 31.8°, 32.2°, 32.9° and 38.4° (2θ) indicating its crystalline nature.[68] In the diffractogram of formulation Ca-IHS4, some of drug sharp peaks disappeared which might suggest a certain loss of drug's crystallinity due to its dispersion within the formulation. Similar results were obtained by Qin et al.[69] Also, the XRD of the formulation revealed the absence of some sharp peaks belonging to the processed ingredients. This observation suggested the decreased crystallinity of the formulation, which runs in accordance with the calculated CI value of TONFC compared to that of the selected formulation (76% and 72.55%, respectively). However, some sharp peaks appeared in the formulation's diffractogram in different positions compared to the individual constituents, which might be due to the formation of some crystallographic planes.

Scanning Electron Microscope (SEM)

As shown in Figure 6, the photograph of the selected in-situ scaffold (Ca-IHS4) showed a clear porous structure, which might be due to the matrix erosion occurring by penetration of the used media within the formed scaffolds while keeping

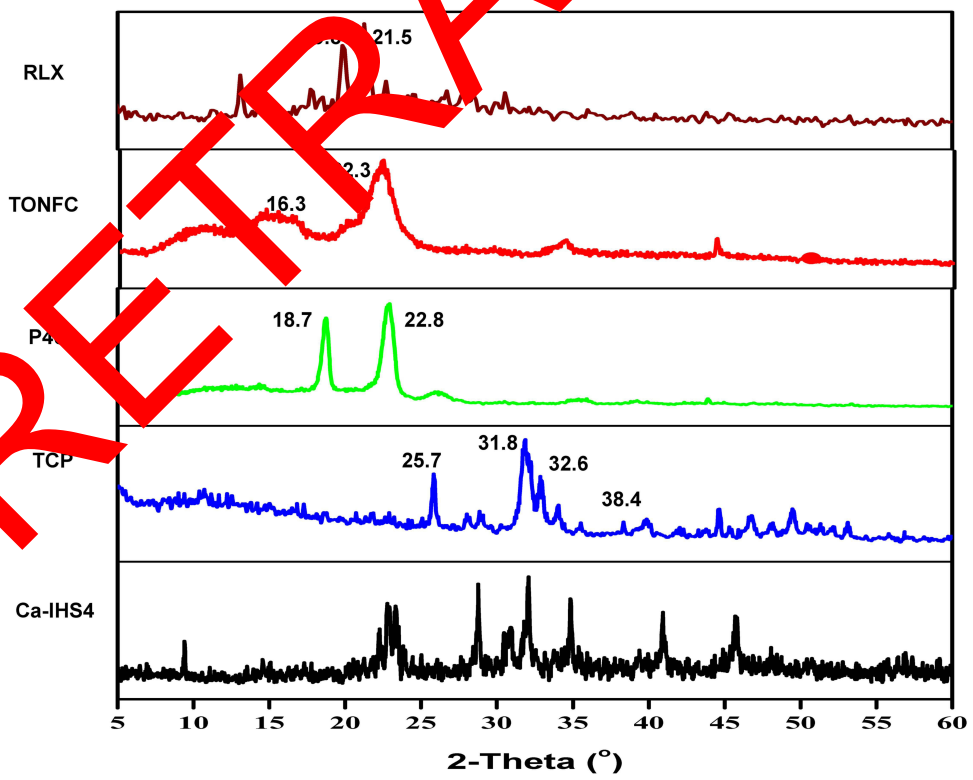

Figure 5 X-ray diffractograms of the investigated samples. Some of drug sharp peaks disappeared in the diffractogram of formulation Ca-IHS4 suggesting a certain loss of drug's crystallinity.

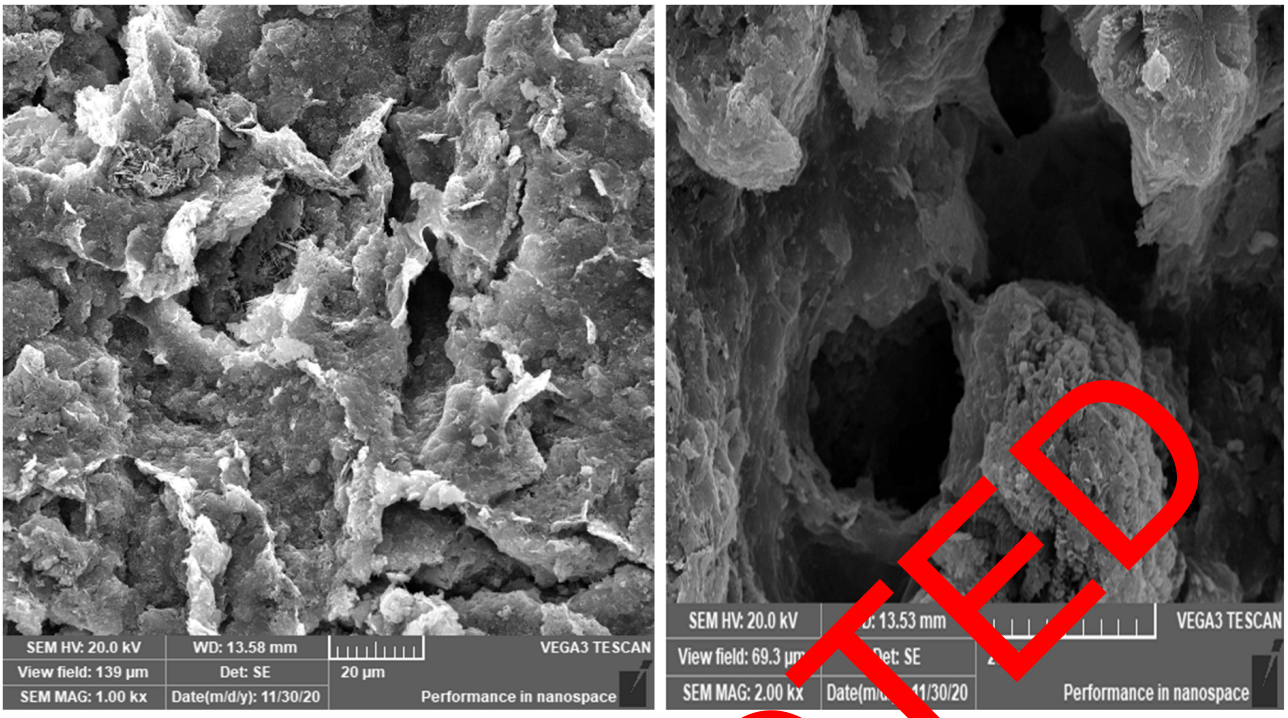

Figure 6 SEM micrographs of the cross sectional view of the selected formulation Ca-IHS4. The micrographs show the porous structure of the formed scaffolds.

of a three-dimensional structure. This photograph indicated the successful in-situ formation of a non-decaying scaffold after subjecting the prepared hydrogel to the release experiment conditions, which mimic the physiological c...

Cytocompatibility Studies

Assessment of Cytotoxicity Applying the ...bility Assay

In this study, the effect of the investigated samples; RLX, Ca-IHS4 and non-medicated Ca-IHS4 (the same composition of the selected formulation Ca-IHS4 without the addition of the drug) on the viability of Saos-2 cells was assessed compared to control cells applying MTT colorimetric assay.[70]

From Figure 7, it can be noticed that all the examined samples boosted the cellular proliferation significantly ($p<0.05$) in a concentration-dependent manner in comparison to the control at the studied time intervals (7, 14 and 21 days) which excluded any toxicity. A significant increased cell growth ($p<0.5$) was observed with RLX and Ca-IHS4 when compared to the non-medicated formulation at the tested time intervals which might be ascribed to osteoblastic stimulatory effect of the drug.[71]

The enhanced cellular growth of Ca-IHS4 ($p<0.05$) compared to the crude RLX might be credited to the porous construction of the hydrogel scaffold along with the intrinsic properties of its components. The porous structure of the prepared hydrogel scaffold as seen in SEM images is essential for cell migration and infiltration as well as for providing a suitable microenvironment for the transport of nutrients and wastes followed by cellular growth, proliferation and tissues vascularization.[19] The hydrophilicity of CONFC might enhance the cellular adhesion;[72] besides, it was formerly reported that nanocellulose possesses a prominent influence on bone mineralization and proliferation.[73,74] It was stated that P407 was biocompatible and helped in enhancing bone cells proliferation and growth.[75] It is well known that calcium phosphates, ie, TCP possess osteoconductive as well as osteoinductive properties aiding in bone regeneration on the materials surfaces[76] and osteoblastic differentiation.[77,78] Both features are essential in supporting cell adhesion and therefore growth.[76,78] Finally, the enhanced effect of the non-medicated formulation compared to the control might be endorsed to the proper matrix structure and components.

Cell Growth Pattern

The adhesion of the cells to any hydrogel scaffold is a crucial step allowing for cells' proliferation, differentiation and hence, tissue restoration.[79,80] This adhesion is known as focal adhesion and happens through several physiochemical reactions between the cells and the hydrogel scaffold.[81,86]

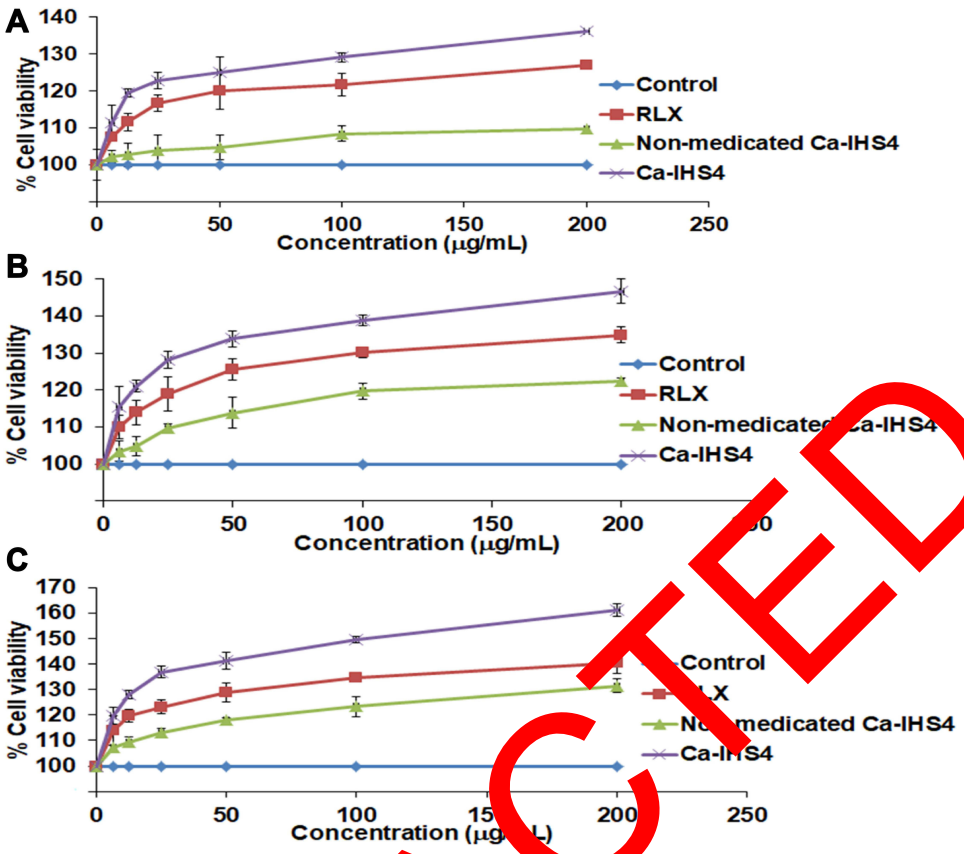

Figure 7 Effect of RLX, Ca-IHS4 and non-medicated Ca-IHS4 on the proli[illegible]s-2 cells after (**A**) 7, (**B**) 14 and (**C**) 21 days. The cellular proliferation effect of Ca-IHS4 was significantly higher ($p<0.05$) than free drug.

The extent of adhesion and interaction between the ce[illegible] and the hydrogel scaffolds was evalua[illegible] by fo[illegible] any change in the fixed cells count appli[illegible] onto [illegible]estigated sample for 21 days at room tempera[illegible]. The extent of cell growth and adhesion was conside[illegible] after [illegible] 14 and 21 days by staining the samples b[illegible] acridine orang[illegible] dye which could stain viable and dea[illegible] cells' nuclei in bright green or red, in that order.

As demo[illegible]rated [illegible] Figure 8, it was noticed that all samples possesse[illegible] better cellular adhesion and growth more t[illegible]n the c[illegible]ntrol at the three time points. Moreover, it was ob[illegible]ed that Ca-IHS4 showed the greatest effect from the pure drug and the non-medicated Ca-IHS4. This effect was enhanced by time, where improved cellular proliferation was observed after 21 days. Besides, the cells propagated in an organized manner with Ca-IHS4. This boosted effect might be attributed to the osteoblastic effect of RLX[71] and the use of TONFC which possesses noticeable role in tissue regeneration as previously stated.[4,82] Additionally, TCP aided in the biomineralization and cell adhesion.[83] The porous structure played a great role in augmenting the cellular adhesion. Again, these results indicated the biocompatibility of the used ingredients along to the biomimetic nature of the prepared hybrid scaffolds as being composed of major bone constituents.[84] The enhanced results of non-medicated Ca-IHS4 compared to the control might be endorsed to the porous structure, which was well correlated to the cell viability results.

Alkaline Phosphatase Assay

Alkaline phosphatase (ALP) enzyme enhances the osteoblastic cells differentiation, propagation and hence bone formation.[85] Hence, determining its concentration in Saos-2 cells cultured with RLX, Ca-IHS4 and non-medicated Ca-IHS4 was assessed to monitor the active bone formation as presented in Figure 9A.

All samples boosted significantly the ALP concentration more than the control ($p < 0.05$) at all-time intervals. Additionally, it could be observed that Ca-IHS4 and crude RLX showed more enhanced improvement in ALP expression compared to the non-medicated Ca-IHS4 ($p < 0.05$) at all-time points, which might be ascribed to the effect of RLX in increasing the bone mineralization, differentiation and density.[4,86] Moreover, the enhanced effect of Ca-IHS4 ($p <$

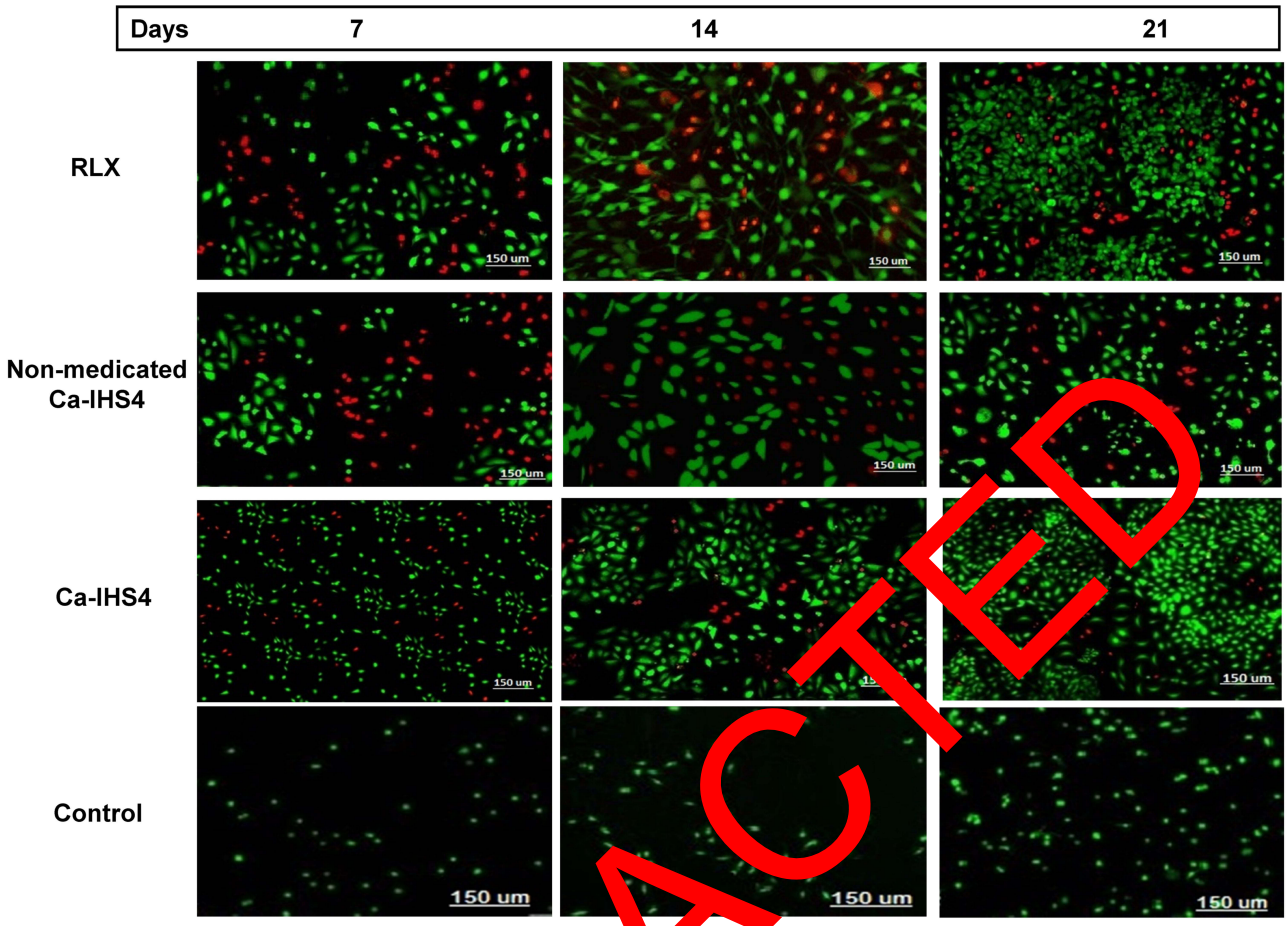

Figure 8 Fluorescence microscope images for Saos-2 cells treated with pure RLX, non-medicated Ca-IHS4 and Ca-IHS4 after 7, 14 and 21 days. Formulation Ca-IHS4 showed the highest cellular adhesion and growth compared to the free drug and the non-medicated Ca-IHS4. Maximum effect was observed after 21 days.

0.05) compared to RLX at the examined time intervals might be endorsed to the porous matrix necessary for concentrating ALP followed by cellular differentiation and proliferation.[4,72,87,88] Additionally, the presence of TONFC and P407 aided in cellular growth as previously mentioned. On the other hand, the addition of TCP might be responsible for osteoblastic differentiation via up-regulating the ALP expression.[89] Furthermore, combining P407 and TONFC along with TCP succeeded to provide an injectable 3D matrix with convenient physical properties able to act as a bone substitute.

The enhanced ALP expression observed with the non-medicated Ca-IHS4 might be ascribed to the porous 3D structure of the prepared hydrogel scaffolds.

Calcium Ion Concentration Assay

Calcium ion is essential for active bone mineralization and formation.[4,91] Results showing the effect of the examined samples cultured on Saos-2 cells on the calcium ion concentration are demonstrated in Figure 9B.

It could be observed that all the samples showed enhanced calcium ion concentrations ($p<0.05$) compared to the control at the examined time intervals. Formulation Ca-IHS4 showed enhanced effect compared to the crude RLX ($p<0.05$) which might be related to the porous 3D matrix of the hydrogel scaffold, which stimulated calcium deposition[92] as well as the enrichment of the formulation with calcium phosphate (TCP). Calcium ions improve bone regeneration through calcification and enhanced cellular signaling via the production of nitric oxide[93] besides enhancing the osteoblastic life span and regulating the osteoblastic functions.[94] In addition, phosphate ions enhance osteoblasts differentiation and growth[95] as well as inhibit osteoclast differentiation.[96]

Furthermore, it was noticed that the non-medicated Ca-IHS4 enhanced calcium ion deposition by time ($p<0.05$) which might be ascribed to the composition as well as the porous structure of hydrogel scaffolds.

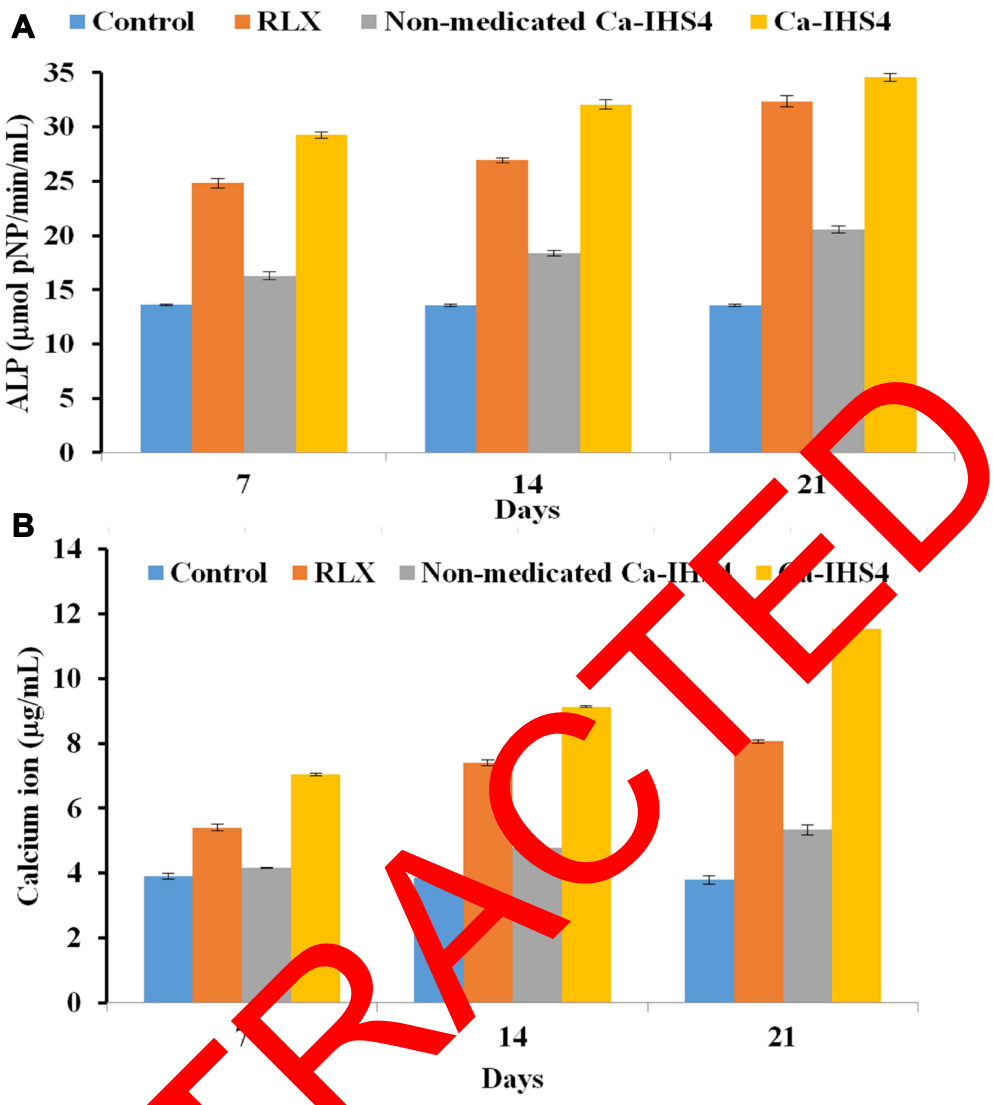

Figure 9 The effect of the tested samples on (**A**) ALP and (**B**) calcium ion concentrations against Saos-2 cells after 7, 14 and 21 days. Formulation Ca-IHS4 boosted significantly the ALP and calcium ion concentrations ($p < 0.05$) compared to free RLX.

From the previous results, it could be concluded that the results of ALP expression activity and that of the calcium ion deposition results were well related, indicating the suitability of the used drug as well as the other components used in the fabrication process of the hydrogel scaffolds.

Conclusion

In the present study, an agro-waste product was treated to prepare cellulose nanofibers (TONFC) which were utilized as a pharmaceutical ingredient based on its benign properties like safety, biodegradability and good mechanical properties. Calcium-enriched in-situ forming hydrogel scaffolds loaded with raloxifene hydrochloride were fabricated applying the cold method using Poloxamer 407 (P407) as a smart thermosensitive polymer in combination with TONFC. The prepared TONFC showed a fibrous structure formed from interconnecting fibers, which were 10–20 nm in diameter and several microns in length. Two sources of calcium were tried; dicalcium phosphate (DCP) and tricalcium phosphate (TCP) were utilized for the scaffolds fabrication aiming at enhancing the bone restoration activity. The formulation fabricated using TONFC in addition to 15% P407 and 10% w/w TCP possessed good injectable properties as well as the most sustained drug release properties with reduced burst effect. Additionally, the in-situ formed scaffolds possessed a porous structure formed owing to the matrix erosion by the penetration of the used media.

The formed scaffolds were biocompatible with excellent ability to enhance cell proliferation of Saos-2 cell line due to enhanced cell adhesion as well as improved ALP activity and boosted calcium ion deposition, suggesting a safe, propitious and effective solution for bone tissue restoration without the need of surgical intervention.

Acknowledgments

The authors would like to acknowledge the role and support of Dr AbdelFattah A. Abdelkhalek, Department of Microbiology of Supplementary General Science, Faculty of Oral & Dental Medicine, Future University in Egypt, Cairo, Egypt, for performing the biological evaluation involving the cytocompatibility studies is highly appreciated.

Funding

This work was supported by the National Research Centre, Cairo, Egypt (grant agreement no. 12010109).

Disclosure

The authors report no conflicts of interest in this work.

References

1. Kamel R, El-Wakil NA, Dufresne A, Elkasabgy NA. Nanocellulos from an agricultural waste to a valuable pharmaceutical ingredien *Int J Biol Macromol*. 2020;163:1579–1590.
2. Kamel R, El-Wakil NA, Abdelkhalek AA, Elkasab NA. Topical cellulose nanocrystals-stabilized nanoemulgel load with ci oflox-acin HCl with enhanced antibacterial activity an issue re ative properties. *J Drug Deliv Sci Technol*. 2021;6 102
3. Slaughter BV, Khurshid SS, Fisher Z, Khade osseini A, Peppas NA. Hydrogels in regener medicine. *Mater*. 2009;21(32-33):3307–3329.
4. Kamel R, El-Wakil NA, Abdelkhalek A Elkasabgy NA. Nanofibrillated cellulose/cy dextrin based 3D caffolds loaded with raloxifene hydroch ide for one regeneration. *Int J Biol Macromol*. 2020;156:70 716.
5. Valo H, Arola S, Laakson P al. Drug re ase from nanoparticles embedded in f ifferent nofibrill cellulose aerogels. *Eur J Pharm Sci*. 13;50 69–77.
6. Liu Y, Lu D, Wang Hierarchi structures of bone and bioinspired bon issue e *Small*. 2016;12(34):4611–4632.
7. Adel IM, ElM MF, Abdelkhalek AA, Elkasabgy NA. Design and characterization highly porous curcumin loaded freeze-dried wafers for wound h ng. *Eur J Pharm Sci*. 2021;25:105888.
8. Griffin M, Kalaskar D, Seifalian A, Butler P. Suppl-3, M4: an update on the application of nanotechnology in bone tissue engineering. *Open Orthop J*. 2016;10:836.
9. Walmsley GG, McArdle A, Tevlin R, et al. Nanotechnology in bone tissue engineering. *Nanomedicine*. 2015;11(5):1253–1263.
10. Faraji AH, Wipf P. Nanoparticles in cellular drug delivery. *Bioorg Med Chem*. 2009;17(8):2950–2962.
11. Kong G, Braun RD, Dewhirst MW. Hyperthermia enables tumor-specific nanoparticle delivery: effect of particle size. *Cancer Res*. 2000;60(16):4440–4445.
12. Edmundson M, Thanh NT, Song B. Nanoparticles based stem cell tracking in regenerative medicine. *Theranostics*. 2013;3(8):573.
13. Jendelová P, Herynek V, DeCroos J, et al. Imaging the fate of implanted bone marrow stromal cells labeled with superparamagnetic nanoparticles. *Magn Resonance Med*. 2003;50(4):767–776.
14. Kleinman HK, Philp D, Hoffman MP. Role of the extracellular matrix in morphogenesis. *Curr Opin Biotechnol*. 2003;14(5):526–532.
15. Kim K, Fisher JP. Nanoparticle technology in bone tissue engineering. *J Drug Target*. 2007;15(4):241–252.
16. Ratner BD, Bryant SJ. Biomaterials: where we have been and where we are going. *Annu Rev Biomed Eng*. 2004;6:41–75.
17. Cui F-Z, Li Y, Ge J. Self-assembly of mineralized collagen composites. *Mater Sci Eng R Rep*. 2007;57(1–6):1–27.
18. Patel M, Fisher JP. Biomaterial scaffolds in pediatric tissue engineering. *Pediatr Res*. 2008;63(5):497.
19. Elkasabgy NA, Mahmoud AA. Fabrication strategies of scaffolds for delivering active ingredients for tissu gineering. *AAPS PharmSciTech*. 2019;20(7):256.
20. Elkasabgy NA, Mahmoud AA, Maged 3D printing: an pealing route for customized drug delivery systems. *I Pharm*. 2020; 3:119732.
21. Jones AC, Milthorpe B, Aver k H, et al. Analysis of 3D bone ingrowth into polymer sca ds via micro mpu tomography imaging. *Biomaterials*. 2 4;25(20): 47–4954.
22. Kim HK, Shim WS, Ki E, et al. Injectable in situ–forming pH/thermo-sensitive h rogel f one tissue gineering. *Tissue Eng Part A*. 2009;1 :923–933.
23. Wu G, Feng , n J, et al. In controlled release of stromal cell-derived factor-1 nd antimiR-138 for on-demand cranial bone regeneration. *Carbohyd olym*. 2018;182:215–224.
24. Sil R, Fabry B, Boccacc AR. Fibrous protein-based hydrogels f cell encapsulation. *Biomaterials*. 2014;35(25):6727–6738.
25. el-Gariepy E, eroux JC. In situ-forming hydrogels–review of t perature-sens e systems. *Eur J Pharm Biopharm*. 2004;58 (2) –426.
26. Elela M , ElKasabgy NA, Basalious EB. Bio-shielding in situ ing gels (BSIFG) loaded with lipospheres for depot injection of qu apine fumarate: in vitro and in vivo evaluation. *AAPS PharmSciTech*. 2017;18(8):2999–3010.
27. Veyries ML, Couarraze G, Geiger S, et al. Controlled release of vancomycin from poloxamer 407 gels. *Int J Pharm*. 1999;192 (2):183–193.
28. Paavola A, Kilpelainen I, Yliruusi J, Rosenberg P. Controlled release injectable liposomal gel of ibuprofen for epidural analgesia. *Int J Pharm*. 2000;199(1):85–93.
29. Wenzel JG, Balaji KS, Koushik K, et al. Pluronic F127 gel formulations of deslorelin and GnRH reduce drug degradation and sustain drug release and effect in cattle. *J Control Release*. 2002;85(1–3):51–59.
30. Zhang L, Parsons DL, Navarre C, Kompella UB. Development and in-vitro evaluation of sustained release poloxamer 407 (P407) gel formulations of ceftiofur. *J Control Release*. 2002;85(1–3):73–81.
31. Kamel R, Basha M, El Awdan S. Development and evaluation of long-acting epidural "smart" thermoreversible injection loaded with spray-dried polymeric nanospheres using experimental design. *J Drug Targ*. 2013;21(3):277–290.
32. Gou M, Li X, Dai M, et al. A novel injectable local hydrophobic drug delivery system: biodegradable nanoparticles in thermo-sensitive hydrogel. *Int J Pharm*. 2008;359(1–2):228–233.
33. Morello KC, Wurz GT, DeGregorio MW. Pharmacokinetics of selective estrogen receptor modulators. *Clin Pharmacokinet*. 2003;42(4):361–372.
34. Patil PH, Belgamwar VS, Patil PR, Surana SJ. Enhancement of solubility and dissolution rate of poorly water soluble raloxifene using microwave induced fusion method. *Braz J Pharm Sci*. 2013;49(3):571–578.
35. Abdel-Salam FS, Elkheshen SA, Mahmoud AA, et al. In-situ forming chitosan implant-loaded with raloxifene hydrochloride and bioactive glass nanoparticles for treatment of bone injuries: formulation and biological evaluation in animal model. *Int J Pharm*. 2020;5 80:119213.

36. Elkasabgy NA, Abdel-Salam FS, Mahmoud AA, et al. Long lasting in-situ forming implant loaded with raloxifene HCl: an injectable delivery system for treatment of bone injuries. *Int J Pharm*. 2019;571:118703.
37. Upadhyay R. Role of calcium bio-minerals in regenerative medicine and tissue engineering. *J Stem Cell Res Ther*. 2017;2(6):166–175.
38. Boskey A, Bullough P, Vigorita V, Di Carlo E. Calcium-acidic phospholipid-phosphate complexes in human hydroxyapatite-containing pathologic deposits. *Am J Pathol*. 1988;133(1):22.
39. Bose S, Tarafder S. Calcium phosphate ceramic systems in growth factor and drug delivery for bone tissue engineering: a review. *Acta Biomater*. 2012;8(4):1401–1421.
40. Jeong J, Kim JH, Shim JH, Hwang NS, Heo CY. Bioactive calcium phosphate materials and applications in bone regeneration. *Biomater Res*. 2019;23(1):1–11.
41. LeGeros RZ. Calcium phosphate-based osteoinductive materials. *Chem Rev*. 2008;108(11):4742–4753.
42. Teixeira S, Rodriguez M, Pena P, et al. Physical characterization of hydroxyapatite porous scaffolds for tissue engineering. *Mater Sci Eng*. 2009;29(5):1510–1514.
43. Ramesh N, Moratti SC, Dias GJ. Hydroxyapatite–polymer biocomposites for bone regeneration: a review of current trends. *J Biomed Mater Res B Appl Biomater*. 2018;106(5):2046–2057.
44. FUJI-CHEMICAL-INDUSTRY-CO.LTD. Fujicalin®. Available from: http://www.fujichemical.co.jp/english/newsletter/newsletter_pharma_0712.html. Accessed December 23, 2020.
45. Saito T, Kimura S, Nishiyama Y, Isogai A. Cellulose nanofibers prepared by TEMPO-mediated oxidation of native cellulose. *Biomacromolecules*. 2007;8(8):2485–2491.
46. Schmolka IV. Artificial skin. I. Preparation and properties of pluronic F-127 gels of treatment of burns. *J Biomed Mater Res*. 1972;6:571–582.
47. Wei G, Xu H, Ding PT, Li SM, Zheng JM. Thermosetting g[illegible] modulated gelation temperature for ophthalmic use: the rheologi[illegible] and gamma scintigraphic studies. *J Control Release*. 2002;83(1):65–74.
48. Kwon KW, Park MJ, Hwang J, Char K. Effects of [illegible] addition [illegible] gelation in aqueous solution of poly(ethylene [illegible]ide)-po[illegible]propyle[illegible] oxide)-poly(ethylene oxide) triblock copol[illegible]mer. *Polym J*. 2001;33(5):404–410.
49. Yu GE, Deng Y, Dalton S, et al. Mice[illegible]ation an[illegible]iation of triblock copoly (oxyethylene oxypropylen[illegible]xyethylene), [illegible]. *J Chem Soc Faraday Trans*. 1992;88(17):2[illegible]–25[illegible].
50. Rawlins EA. Rheology. In: Careless JE, [illegible]itor. *Bentley's Textbook of Pharmaceutics*. London, [illegible]ngland: Bailliére [illegible]ndall; 1977:123–139.
51. Leroux L, Hatim Z, F[illegible]ne M, Lacout J. Effect[illegible] of various adjuvants (lactic acid, glycer[illegible] and chit[illegible]n) on the injectability of a calcium phosphate cement. *B[illegible]*. 1[illegible]9;25(2):31S–34S.
52. Mahmoud A[illegible] Elkasa[illegible] NA, Abd[illegible]halek AA. Design and characterizati[illegible] of [illegible]ulsified [illegible]spray[illegible]ried alginate microparticles as a carr[illegible] for the [illegible]ually actin[illegible]rug roflumilast. *Eur J Pharm Sci*. 2018;[illegible]2:64–7[illegible].
53. Korsmeyer [illegible], Gurny R, Doelker E, Buri P, Peppas N. Mechanisms of potassium [illegible]oride release from compressed, hydrophilic, polymeric matrices: effect [illegible]entrapped air. *J Pharm Sci*. 1983;72(10):1189–1191.
54. Peppas N. Analysis of Fickian and Non-Fickian Drug Release from Polymers. *Pharm Acta Helv*. 1985;60(4):110–111.
55. Segal L, Creely J, Martin A Jr, Conrad C. An empirical method for estimating the degree of crystallinity of native cellulose using the X-ray diffractometer. *Textile Res J*. 1959;29(10):786–794.
56. Heerspink W, Hafkenscheid J, Siepel H, van der Ven-Jongekryg J, Dijt C. Temperature-converting factors for enzymes: comparison of methods. *Enzyme*. 1980;25:333–341.
57. Ishikawa K, Miyamoto Y, Takechi M, et al. Non-decay type fast-setting calcium phosphate cement: hydroxyapatite putty containing an increased amount of sodium alginate. *J Biomed Mater Res*. 1997;36(3):393–399.
58. Martin A. *Physical Pharmacy: Physical Chemical Principles in the Pharmaceutical Sciences*. BI Waverly. Pvt Ltd; 1993.
59. Paul S, Egbert J, Walsh A, Hoey M. Pressure measurements during injection of corticosteroids. *Med Biol Eng Comput*. 1998;36(6):729–733.
60. Sigma-Aldrich. Hydroxyapatite. Available from: https://www.sigmaaldrich.com/catalog/product/aldrich/900203?lang=en&region=EG&cm_sp=Insite-_-caSrpResults_srpRecs_srpModel_hydroxyapatite-_-srpRecs3-3. Accessed December 23, 2020.
61. Bohner M, Baroud G. Injectability of calcium phosphate pastes. *Biomaterials*. 2005;26(13):1553–1563.
62. Montufar E, Maazouz Y, Ginebra M. Relevance of the setting reaction to the injectability of tricalcium phosphate pastes. *Acta Biomater*. 2013;9(4):6188–6198.
63. O'Neill R, McCarthy H, Montufa[illegible], et al. C[illegible]ical review: injectability of calcium phosphate [illegible]tes and cemen[illegible]. *Acta Biomater*. 2017;50:1–19.
64. Nakata R, Tachibana A, [illegible]nabe T. [illegible]paration o[illegible]keratin hydrogel/hydroxyapatite compo[illegible]e and its eva[illegible]ion [illegible]a controlled drug release carrier. *Mat[illegible] Sci Eng*. [illegible]14;41:59[illegible].
65. Bose S, Tarafder S, [illegible]aging[illegible] J, Bandyopadhyay A. Calcium phosphate ceramic[illegible]n drug [illegible]very. *Jom*. [illegible]011;63(4):93–98.
66. Sato H, M[illegible]gawa Y, Oka[illegible]T, M[illegible]ajima M, Sunada H. Dissolution mecha[illegible]m o[illegible]iclofenac sodi[illegible]rom wax matrix granules. *J Pharm Sci*. 1997;86(8):[illegible]9–934.
67. Ni[illegible]yama Y, Sugiy[illegible]a J, Chanzy H, Langan P. Crystal structure and hydrogen bonding syst[illegible]n in cellulose Iα from synchrotron X-ray and neutron fiber diffraction. *J Am Chem Soc*. 2003;125(47):14300–14306.
68. Londoño-R[illegible]repo SM, Jeronimo-Cruz R, Millán-Malo BM, Rivera-Muñoz EM, [illegible]odriguez-García ME. Effect of the nano crystal size on [illegible] X-ray [illegible]diffraction patterns of biogenic hydroxyapatite from human, bovine, and porcine bones. *Sci Rep*. 2019;9(1):1–12.
69. Qin L, Zhao X, He Y, et al. Preparation, characterization, and in vitro [illegible]aluation of resveratrol-loaded cellulose aerogel. *Materials*. 2020;13(7):1624.
70. Mosmann T. Rapid colorimetric assay for cellular growth and survival: application to proliferation and cytotoxicity assays. *J Immunol Methods*. 1983;65(1–2):55–63.
71. Taranta A, Brama M, Teti A, et al. The selective estrogen receptor modulator raloxifene regulates osteoclast and osteoblast activity in vitro. *Bone*. 2002;30(2):368–376.
72. Bacakova L, Filova E, Parizek M, Ruml T, Svorcik V. Modulation of cell adhesion, proliferation and differentiation on materials designed for body implants. *Biotechnol Adv*. 2011;29(6):739–767.
73. Patel DK, Seo Y-R, Dutta SD, Lim K-T. Enhanced osteogenesis of mesenchymal stem cells on electrospun cellulose nanocrystals/poly (ε-caprolactone) nanofibers on graphene oxide substrates. *RSC Adv*. 2019;9(62):36040–36049.
74. Lin N, Dufresne A. Nanocellulose in biomedicine: current status and future prospect. *Eur Polym J*. 2014;59:302–325.
75. Liu H, Li W, Liu C, et al. Incorporating simvastatin/poloxamer 407 hydrogel into 3D-printed porous Ti6Al4V scaffolds for the promotion of angiogenesis, osseointegration and bone ingrowth. *Biofabrication*. 2016;8(4):045012.
76. Albrektsson T, Johansson C. Osteoinduction, osteoconduction and osseointegration. *Eur Spine J*. 2001;10(2):S96–S101.
77. Ambard AJ, Mueninghoff L. Calcium phosphate cement: review of mechanical and biological properties. *J Prosthodont*. 2006;15(5):321–328.
78. Samavedi S, Whittington AR, Goldstein AS. Calcium phosphate ceramics in bone tissue engineering: a review of properties and their influence on cell behavior. *Acta Biomater*. 2013;9(9):8037–8045.
79. Hunt NC, Grover LM. Cell encapsulation using biopolymer gels for regenerative medicine. *Biotechnol Lett*. 2010;32(6):733–742.

80. Agrawal CM, Ray RB. Biodegradable polymeric scaffolds for musculoskeletal tissue engineering. *J Biomed Mater Res*. 2001;55(2):141–150.
81. Chang H-I, Wang Y. *Cell Responses to Surface and Architecture of Tissue Engineering Scaffolds. Regenerative Medicine and Tissue Engineering-Cells and biomaterials*. InTechOpen; 2011.
82. Lou Y-R, Kanninen L, Kuisma T, et al. The use of nanofibrillar cellulose hydrogel as a flexible three-dimensional model to culture human pluripotent stem cells. *Stem Cells Dev*. 2014;23(4):380–392.
83. Kamitakahara M, Ohtsuki C, Miyazaki T. Behavior of ceramic biomaterials derived from tricalcium phosphate in physiological condition. *J Biomater Appl*. 2008;23(3):197–212.
84. Ma X, He Z, Han F, Zhong Z, Chen L, Li B. Preparation of collagen/hydroxyapatite/alendronate hybrid hydrogels as potential scaffolds for bone regeneration. *Colloids Surf B Biointerfaces*. 2016;143:81–87.
85. Golub EE, Boesze-Battaglia K. The role of alkaline phosphatase in mineralization. *Curr Opin Orthop*. 2007;18(5):444–448.
86. Kavas A, Cagatay ST, Banerjee S, Keskin D, Tezcaner A. Potential of Raloxifene in reversing osteoarthritis-like alterations in rat chondrocytes: an in vitro model study. *J Biosci*. 2013;38(1):135–147.
87. Salerno A, Di Maio E, Iannace S, Netti P. Tailoring the pore structure of PCL scaffolds for tissue engineering prepared via gas foaming of multi-phase blends. *J Porous Mater*. 2012;19(2):181–188.
88. Hollister SJ. Porous scaffold design for tissue engineering. *Nat Mater*. 2005;4(7):518–524.
89. Liu J, Zhao L, Ni L, et al. The effect of synthetic α-tricalcium phosphate on osteogenic differentiation of rat bone mesenchymal stem cells. *Am J Transl Res*. 2015;7(9):1588.
90. Orimo H. The mechanism of mineralization and the role of alkaline phosphatase in health and disease. *J Nippon Med School*. 2010;77(1):4–12.
91. Elkasabgy NA, Mahmoud AA, Shamma RN. Determination of cytocompatibility and osteogenesis properties of in situ forming collagen-based scaffolds loaded with bone synthesizing drug for bone tissue engineering. *Int J Poly Mater Poly Biomater*. 2018;67(8):494–500.
92. Whitehead MA, Fan D, Mukherjee P, Akkaraju GR, Canham LT, Coffer JL. High-porosity poly (ε-caprolactone)/mesoporous silicon scaffolds: calcium phosphate deposition and biological response to bone precursor cells. *Tissue Eng Part A*. 2008;14(1):195–206.
93. Riddle RC, Taylor AF, Genetos DC, Donahue HJ. MAP kinase and calcium signaling mediate fluid flow-induced human mesenchymal stem cell proliferation. *Am J Physiol Cell Physiol*. 2006;290(3):C776–C784.
94. Kuroda Y, Hisatsune C, Nakamura T, Matsuo K, Tokoshiba K. Osteoblasts induce Ca2+ oscillation-independent NFAT1 activation during osteoclastogenesis. *Proc Natl Acad Sci*. 2008;105(25):8643–8648.
95. Julien M, Khoshniat S, Lacreuse A, et al. Phosphate-dependent regulation of MGP in osteoblasts: role of ERK1/2 and Fra-1. *J Bone Mineral Res*. 2009;24(11):1856–1868.
96. Mozar A, Haren N, Chasseraud M, et al. High extracellular inorganic phosphate concentration inhibits RANK–RANKL signaling in osteoclast-like cells. *J Cell Physiol*. 2008;215(1):47–54.